Monthly Notices
of the
ROYAL ASTRONOMICAL SOCIETY

MNRAS **480,** 3503–3510 (2018)
Advance Access publication 2018 July 18

doi:10.1093/mnras/sty1887

OH 18 cm observations of the intermediate-velocity molecular cloud G211+63

Allison J. Smith,[1]★ Loris Magnani,[1] Louis Gonzalez[2] and Timothy Robishaw[3]

[1]*Department of Physics and Astronomy, University of Georgia, Athens, GA 30602, USA*
[2]*Department of Physics and Astronomy, Georgia State University, Atlanta, GA 30302, USA*
[3]*National Research Council Canada, Herzberg Astronomy and Astrophysics Programs, Dominion Radio Astrophysical Observatory, Penticton, BC V2A 6J9, Canada*

Accepted 2018 July 10. Received 2018 June 28; in original form 2018 May 11

ABSTRACT

We detected OH 18 cm main line emission from 5 of 7 positions in the intermediate-velocity molecular cloud (IVMC) G211+63. These are the first detections of hydroxyl in IVMCs. Our OH detections at A_V levels ranging from 0.24 to 0.27 mag reinforce the notion that these lines can efficiently trace diffuse, low-extinction molecular gas. N(OH) is derived for a range of excitation temperatures (5–30 K) and likely falls between 1 and 16 $\times$ 10^{13} cm^{-2}. The corresponding $N(H_2)$ values are consistent both with estimates derived from $E(B-V)$ and CO data. Estimates of the cloud mass from the OH data range from 26 to 820 $M_\odot$ for distances from 100 to 400 pc and T_{ex} from 5 to 10 K. These values are 3–20 times less than the virial mass of the cloud. It is likely IVMCs resemble high-latitude clouds in this respect. If so, they are transient structures breaking up on time-scales of $\sim 10^6$ yr.

Key words: ISM: clouds – ISM: molecules.

1 INTRODUCTION

The high-latitude molecular clouds were identified as a distinct population by Magnani, Blitz & Mundy (1985). Among the list of 57 objects identified at $|b| \geq 30^\circ$ was the Draco molecular cloud (see also Mebold et al. 1985), an object that has a Local Standard of Rest (LSR) velocity ~ -25 km s^{-1}, 4σ from the average velocity of the cloud ensemble (average $v_{LSR} \approx 0$ km s^{-1}; dispersion ≈ 6 km s^{-1}; Magnani, Hartmann & Speck 1996). The Draco molecular cloud was the first example of an intermediate-velocity *molecular* cloud (IVMC). We stress here that the clouds we are discussing are *not* the intermediate-velocity lines of sight detected in H_2 absorption by Richter et al. (2003) and Wakker (2006) using the Far Ultraviolet Spectroscopic Explorer (FUSE). Those lines of sight all have $N(H_2)$ levels less than 10^{17} cm^{-2} and are *atomic* intermediate-velocity clouds (IVCs) with molecules detectable only via absorption lines at relatively low column densities compared to typical molecular clouds. By IVMCs we mean objects at $|b| \geq 30^\circ$ with CO(1–0) emission at 115 GHz that resemble diffuse and translucent molecular clouds (see van Dishoeck & Black 1988).

In addition to the Draco cloud, only six other IVMCs are known. Two were found by Heiles, Reach & Koo (1988) and partially mapped in the CO(1–0) line by Reach, Koo & Heiles (1994). Three more IVMCs were identified by Magnani & Smith (2010) and are located in a 12° × 4° region near a large, atomic IVC dubbed the intermediate-velocity spur. This object is believed to extend into the Galactic halo (Kuntz & Danly 1996) so that the three IVMCs may be halo or, at least, thick disc objects. None of these three objects have been mapped in any molecular tracer. The final object, G211+63, was discovered during the course of a CO(1–0) survey of high-latitude infrared-excess regions by Désert, Bazell & Blitz (1990). With an LSR velocity of -39 km s^{-1} the cloud is clearly an IVMC. The two molecular detections that were reported in the discovery paper are in an IVC H I complex that was mapped by Verschuur (1971) and Meng & Kraus (1970). No additional CO or other molecular mapping of the cloud exists, but an infrared map shown by Désert, Bazell & Blitz shows a 100 μm structure about 60 arcmin × 60 arcmin in RA and Dec. extent. In Fig. 1, at the left, we show a 3° × 3° $E(B-V)$ map based on the Schlegel, Finkbeiner & Davis (1998) data that shows the cloud and its environs. In the $E(B-V)$ map, the cloud appears somewhat smaller than what is seen in the *IRAS* 100 μm data.

The high-latitude molecular clouds are primarily a population of diffuse and translucent molecular clouds. The two most interesting properties that the clouds share are that they are within a few hundred parsecs of the Sun and that the majority of the clouds are not gravitationally bound and are breaking up on the time-scale of the sound crossing time ($\sim 10^6$ yr). This is very different from the overwhelming majority of molecular clouds that are gravitationally bound and are the sites of star formation. It seems likely that the diffuse and translucent molecular clouds at high Galactic latitude are part of the cold neutral medium and represent the molecular portion of that phase of the ISM. In these objects, turbulence rather

★ E-mail: allison@physast.uga.edu

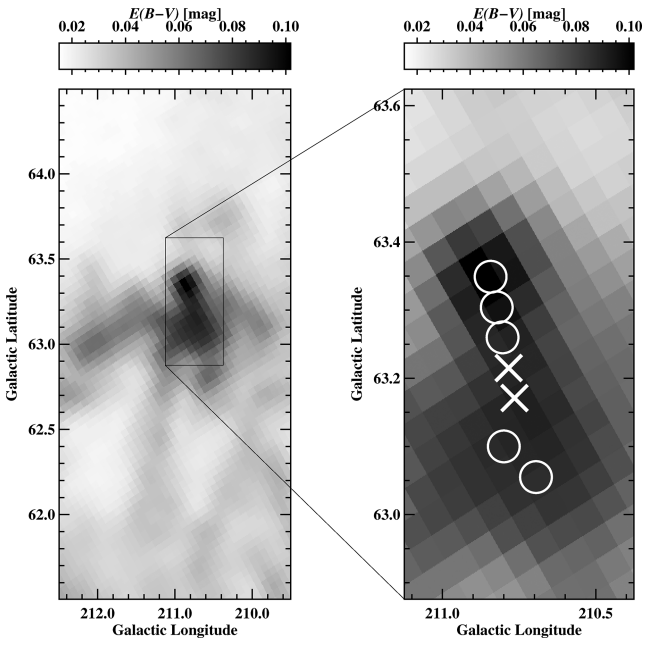

Figure 1. *Left*: Dust map in $E(B-V)$ from Schlegel et al. (1998) centred on IVMC G211+63. $E(B-V)$ is depicted in linear scale from 0.014 to 0.102 mag as shown by the bar at the top. *Right*: Close-up dust map of the cloud in $E(B-V)$ centered on $(\ell, b) = (210.75^\circ, 63.25^\circ)$ showing the lines of sight we observed. $E(B-V)$ is depicted in linear scale in the same manner as the larger region. Detections are depicted by circles with diameter of 3 arcmin (the approximate beam size of the Arecibo radio telescope at 1667 MHz). Each non-detection is represented by an X (however, see the text).

than gravity is the main structuring mechanism (see e.g. Shore et al. 2007).

The IVMCs are a subpopulation of the high-latitude molecular clouds. With the exception of the Draco cloud, which is an anomalous object both among high-latitude molecular clouds and IVMCs (i.e. its cometary morphology, its size compared to the other IVMCs), little is known about these objects. For instance, their gravitational stability has not yet been determined. If they are gravitationally bound, they would resemble the molecular clouds, both large and small, along the Galactic plane. If unbound, then they would be like nearly all of the diffuse and translucent molecular clouds.

A determination of the mass and gravitational state of the IVMCs is the first step in evaluating their role in the molecular inventory of the Galaxy. To date, this has only been done for the anomalous Draco cloud complex. In this paper, we report on observations of the most opaque portion of the infrared object identified by Désert et al. (1990) in the 18 cm OH main lines at 1665 and 1667 MHz in an effort to estimate the molecular mass of the cloud and determine whether or not this IVMC is gravitationally bound.

We discuss the efficacy with which the 1667 MHz OH main line can be used to trace diffuse molecular gas in Section 2 and our observations of the OH main lines in G211+63 in Section 3. We describe our results in Section 4 and determine the mass and gravitational state of the cloud in Section 5. Finally, we summarize our results in Section 6.

2 THE EFFICACY OF THE OH 18 CM LINES FOR TRACING DIFFUSE MOLECULAR GAS

Historically, the CO(1–0) transition has been the workhorse tracer for molecular gas in the Galaxy. However, Grenier, Casandjian & Terrier (2005) proposed that CO may not reliably trace low-density, diffuse molecular gas. They used a combination of gamma-ray and infrared data to determine the amount of H_2 present in the Galaxy, dividing it into CO-detectable and CO-dark portions. Models of photodissociation regions (e.g. Hollenbach & Tielens 1997; Wolfire, Hollenbach & McKee 2010) indicate that in the outer regions of molecular clouds, where the environment is low-density and low-extinction, OH and C^+ should be present in significant quantities. This is confirmed observationally since the CO-dark gas has been detected using the [C II] line at 158 μm (e.g. Langer et al. 2010, 2014), and the OH main lines at 18 cm (Allen et al. 2012). We review here the evidence that the 1665 and 1667 MHz OH lines can be used to trace molecular gas in low-density environments.

More than two decades ago, the case was made by Wannier et al. (1993) that molecular gas not detectable by conventional CO(1–0) mapping could be picked up by OH observations at 1665 and 1667 MHz. Later, Barriault et al. (2010a) and Cotten et al. (2012) came to similar conclusions based on OH observations of high-latitude molecular clouds. Recent work by Allen et al. (2012) and Allen, Hogg & Engelke (2015) implies that the OH 18 cm lines are better tracers than the CO(1–0) transition for diffuse molecular gas – at least for CO-mapping at typical rms levels [e.g. the various surveys that comprise the Dame, Hartmann & Thaddeus (2001) CO(1–0) map of the Galactic plane have rms noise levels ranging over 0.12–0.43 K]. In these low-density, low-extinction regions, the best molecular tracers are the CO(1–0) line (but at better sensitivities and velocity resolutions than for conventional surveys – see Donate & Magnani 2017), the OH 18 cm main lines, and the CH 9 cm main line (e.g. Magnani & Onello 1993 and references therein).

Given the above, a survey for molecular gas in the OH 18 cm main lines at the very least should be as efficient as one in CO(1–0) for detecting diffuse molecular gas. This characteristic of the OH main lines is important because a glance at the Schlegel et al. (1998) dust maps shows that G211+63 has $E(B-V)$ values in the 0.08–0.10 mag range. Detections of molecular emission lines in the radio regimes at $E(B-V)$ levels ∼0.1 mag are at the limit of feasibility with current receiver technology (see discussion in Section 8.4 of Magnani & Shore 2017).

3 OBSERVATIONAL SET-UP AND STRATEGY

The principal observations were made from 2016 July to December with the 305 m radio telescope at the Arecibo Observatory in Puerto Rico[1] using the *L*-band wide receiver. The back end was the wideband Arecibo Pulsar Processor (WAPP) configured to observe simultaneously the two principal OH lines (1665, 1667 MHz), the satellite OH lines (1612, 1720 MHz), and the H I 21 cm line that was in the receiver's band. Each WAPP board registered both polarizations with 1.5625 MHz bandwidth, 9-level sampling, and 2048 channels per spectrum. This provided a resolution of 0.14 km s^{-1} per channel over a bandwidth of 281 km s^{-1} centred at $v_{\rm LSR} = 0$ km s^{-1}. At 1667 MHz, the angular resolution of Arecibo with the *L*-band

[1]During these observations, the Arecibo Observatory was operated by SRI International under a cooperative agreement with the National Science Foundation (AST-1100968), and in alliance with Ana G. Méndez-Universidad Metropolitana, and the Universities Space Research Association.

wide receiver is 2.6 arcmin × 3.1 arcmin elongated in azimuth. System temperatures on the sky at 1.6 GHz were typically 25–32 K and a five minute scan resulted in 1σ rms noise levels per channel of ∼50 mK. The observations were made using only scans on the source with a fifth-order baseline removed from each spectrum.

We observed six positions in the central regions of the G211+63 cloud (see Table 1) as determined from the Schlegel et al. (1998) $E(B-V)$ maps (see Fig. 1, at the right). Each position was observed for periods ranging from 80 to 255 minutes. An additional position (labelled 'H I peak' in Table 1) was observed as part of a separate project to measure the magnetic field in IVCs using the Zeeman effect at 21 cm (Smith 2018). These data were obtained from 2013 May to September again using the Arecibo radio telescope. Although the H I line was the main objective of that project, the OH 18 cm main lines were also observed along with the 1720 MHz satellite line (for the Zeeman project, the 1612 MHz line was omitted). The spectrometer was the Interim 50 MHz Correlator and the bandwidth was 3.125 MHz resulting in a velocity resolution of 0.275 km s^{-1} for the OH 18 cm main lines. This particular line of sight was observed for 25.73 h using on-source scans only with the Stokes parameters recorded for each line. The resulting rms for this spectrum, 2 mK, represents one of the most sensitive observations of the OH 18 cm main lines. Thus, not only did we clearly detect the $F = 2 - 2$ main line at 1667 MHz, but also the $F = 1 - 1$ line at 1665 MHz. With our bandwidth of 3.125 MHz, both lines were actually present on one of the subcorrelator boards and are noticeable in the raw spectrum.

The location of all the observed positions are shown in Fig. 1 (right) superposed on a 0.75° × 0.75° $E(B-V)$ map from the Schlegel et al. (1998) data base centred on G211+63. A_V values for the observed lines of sight are obtained using $R = 3.1$ and range from 0.24 to 0.27 mag. Our detections of the OH 18 cm lines at these extinctions, equivalent to $E(B-V)$ values of ≈ 0.08 mag, represent detections of hydroxyl at some of the lowest dust levels to date.

4 RESULTS

The results of our observations are shown in Table 1. Five of the seven lines of sight resulted in detections. Figs 2(a)–(e) show the spectra of the 1667 MHz line detections. A composite spectrum of the four detections made at 0.27 km s^{-1} resolution after Hann-smoothing is shown in Fig. 3. Three of these positions show two components as does the composite spectrum. This behaviour was also evident in the CO(1–0) line for the position we call 'CO-peak' (Désert et al. 1990; however, see Section 5.2).

4.1 The OH main lines at the H I peak

The OH detection at the H I peak was serendipitous in the sense that the observations were a part of another project whose main goal was to detect Zeeman splitting of the 21 cm H I line (see Smith 2018 for a discussion of those results). Consequently, the observed position is not at the dust peak of the cloud [$E(B-V) \approx 0.09$ mag from the Schlegel et al. (1998) data] but at the bottom of the dust ridge, although the $E(B-V)$ value is only slightly lower there (≈0.08 mag). Nevertheless, it is surprising that the OH emission detected at the H I peak is stronger than that from the other positions along the infrared ridge seen in Fig. 1. Because of the extremely low rms of the observations, an outright detection in the cloud periphery might have been expected given the proven ability of the OH 1667 MHz to trace low-density molecular gas in low extinction regions (see Section 2). However, T_B and W_{OH} at the H I peak are significantly larger than the values for any of the components at the other positions. Given the sensitivity of this observation it is likely that we would have detected OH emission at positions 4 and 5 had we integrated significantly longer. It would be intriguing to map the whole cloud at the 2–3 mK rms level to see just how far OH emission could be detected. However, the long integration times needed for this kind of sensitivity make this idea difficult to implement.

In addition to the 1667 MHz line, we also detected the 1665 MHz line. The parameters are shown in Table 3 and discussed in Section 4.3. The two lines for a composite spectrum of the first four detections in Table 1 are shown in Fig. 3 and at the H I peak are shown in Fig. 4.

4.2 The column density of OH and H_2

We use our observations to determine N(OH) for each detected position in the cloud. For the 18 cm lines, in the optically thin approximation, N(OH) can be expressed as

$$N(\mathrm{OH}) = \frac{C_i W_i(\mathrm{OH})}{F \eta_B} \frac{T_{\mathrm{ex},i}}{T_{\mathrm{ex},i} - T_{\mathrm{bg}}} \ \mathrm{cm}^{-2}, \quad (1)$$

where i represents one of the 18 cm hyperfine lines, C_i is a constant [$= 2.39 \times 10^{14}$ cm^{-2} K^{-1} km^{-1} s for the 1667 MHz line, e.g. Wouterloot 1981], and F is the filling factor of the cloud in the Arecibo beam that we will assume to be 1.0. The beam efficiency, η_B, can be measured at Arecibo by observing bright quasars. Throughout the 2016 observing run η_B varied between 0.57 and 0.78 at 1415 MHz with an average of 0.69 ± 0.07. The beam efficiency decreases with frequency so we used 0.65 ± 0.07 in our calculations. The last factor in equation (1) requires knowledge of the excitation temperature of the transition, T_{ex}, and the background radiation temperature, T_{bg}, at 1.6 GHz. The latter is a combination of the cosmic microwave background radiation, the Galactic synchrotron emission, and the non-thermal background from unresolved radio sources that result in $T_{bg} \approx 3.3$ K (see e.g. Grossmann et al. 1990; Barriault et al. 2010a). If observations of all four lines of the $^2\Pi_{3/2}$ $J = 3/2$ system are available, T_{ex} can be determined explicitly (see e.g. Wouterloot 1981). In our case, the satellite lines are too weak to be detected so we will determine N(OH) for four plausible values of T_{ex}: 5 , 10, 20, and 30 K. The results are shown in Table 2 and range from 1.2 to 15.9 $\times 10^{13}$ cm^{-2} across the temperature range.

To convert N(OH) to $N(H_2)$ requires the OH/H_2 abundance. Lucas & Liszt (1996) quote values of 2.5–5.0 × 10^{-8} for diffuse clouds with extinction similar to that of G211+63 and Liszt & Lucas (2002) obtain $N(\mathrm{OH})/N(H_2) = 1.0 \pm 0.2 \times 10^{-7}$ for lines of sight in diffuse through dark clouds. Most recently, Weselak et al. (2010) derive a molecular column density ratio for OH/H_2 of 1.05 ± 0.14 × 10^{-7} for 16 translucent lines of sight. For the remainder of the paper we will adopt an OH/H_2 ratio for G211+63 of 1.0 × 10^{-7}.

The subsequent range of $N(H_2)$, 1–16 $\times 10^{20}$ cm^{-2}, can be compared with $N(H_2)$ estimated from the extinction and the relationship between $N(H_2)$ and $E(B-V)$ established by Bohlin, Savage & Drake (1978) from observations of diffuse gas in front of early type stars. Using their well-established relation between $N(H_{total})$ [$\equiv 2N(H_2) + N(\mathrm{H\,I})$] and $E(B-V)$, Désert et al. (1990) obtained a value of $1.9 \pm 0.2 \times 10^{20}$ cm^{-2} based on an infrared conversion factor determined by Bloemen et al. (1986). If we use the Bohlin, Savage & Drake relation, $N(H_{total})/E(B-V) = 5.8 \times 10^{21}$ cm^{-2} mag^{-1}, and the average $E(B-V)$ over our lines of

Table 1. Results of OH observations at 1667 MHz for G211+63.

Position	ℓ (deg)	b (deg)	T_A (mK)	Δv(FWHM) (km s^{-1})	$v_{\rm LSR}$ (km s^{-1})	$W^a_{\rm OH}$ (mK km s^{-1})	Integration time (min)	A^b_V (mag)
CO peak[c]	210.800	63.100	11.1 ± 4.3	2.49 ± 0.96	−39.13	29.6 ± 16.2	220	0.242
Position 1[c]	210.843	63.349	23.4 ± 3.8	2.77 ± 0.45	−37.98	64.8 ± 14.9	230	0.274
	–	–	18.1 ± 3.8	4.03 ± 0.85	−41.62	78.0 ± 21.7	–	–
Position 2[c]	210.823	63.304	26.0 ± 3.7	2.55 ± 0.36	−38.43	70.9 ± 13.3	255	0.265
	–	–	18.5 ± 3.7	2.11 ± 0.42	−41.99	41.8 ± 11.0	–	–
Position 3[c]	210.804	63.260	12.6 ± 4.6	5.80 ± 2.12	−40.16	78.1 ± 37.8	190	0.246
Position 4	210.784	63.215	11.0[d]	–	–	–	125	0.244
Position 5	210.765	63.171	10.2[d]	–	–	–	80	0.247
Total four detections[c]	–	–	13.5 ± 1.4	2.78 ± 0.29	−38.38	40.2 ± 5.9	895	–
	–	–	9.9 ± 1.4	2.18 ± 0.31	−42.01	23.1 ± 4.3	–	–
H I peak[e]	210.695	63.055	39.9 ± 2.1	3.45 ± 0.18	−39.31	147.3 ± 10.2	1544	0.238

[a] $W_{\rm OH}$ is defined as $\int T_A\, {\rm d}v$.
[b] Schlafly & Finkbeiner (2011).
[c] Data are Hann-smoothed to 0.27 km s^{-1} resolution.
[d] One sigma rms.
[e] This line of sight was observed with velocity resolution of 0.27 km s^{-1}. No Hann-smoothing was applied.

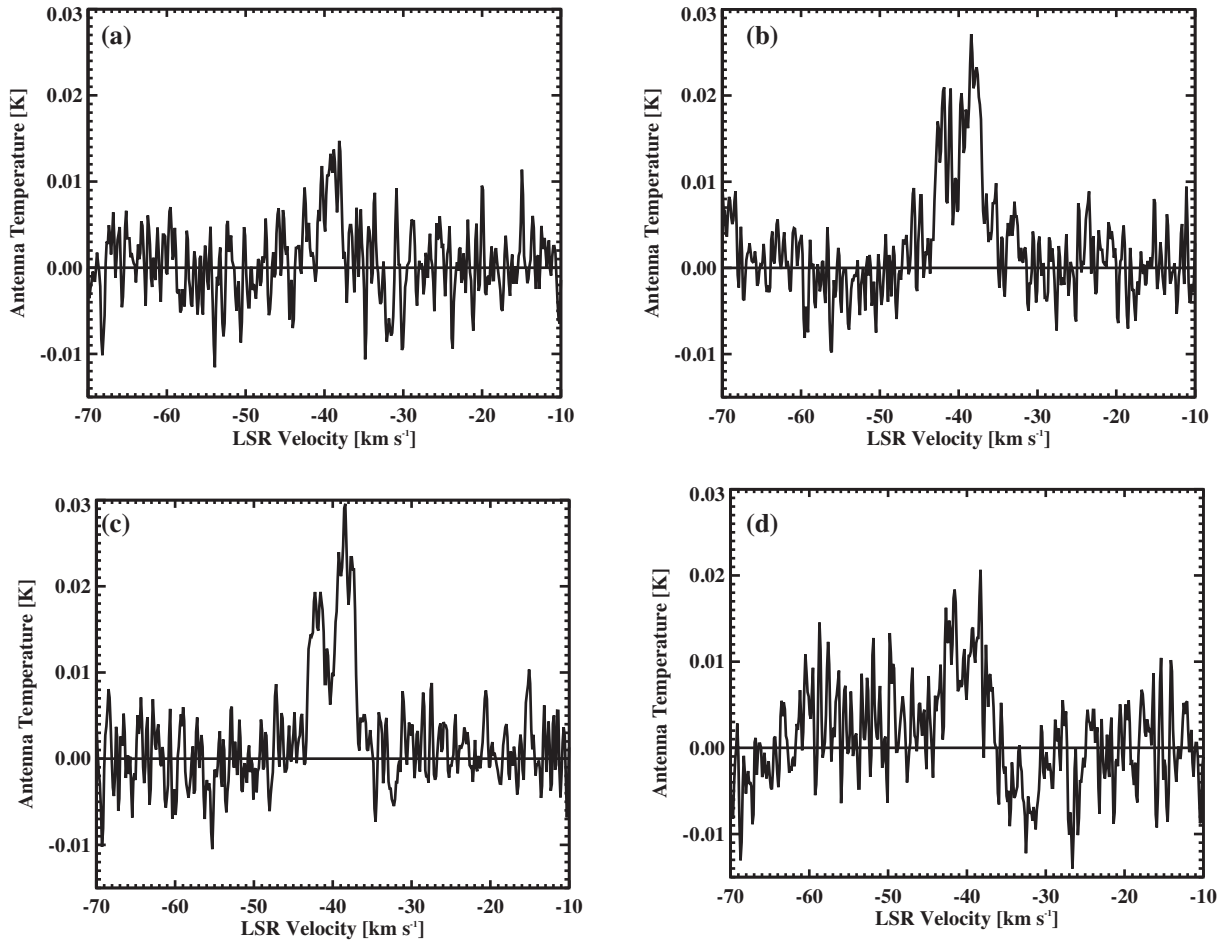

Figure 2. (a) The OH 1667 line for the position 'CO peak' in Table 1. The Gaussian-fit line parameters are also given in Table 1. The data have been Hann-smoothed to a velocity resolution of 0.27 km s^{-1} and the integration time on source was 3.67 h. (b) The OH 1667 line for position 1 in Table 1. The Gaussian-fit line parameters for this detection are also given in Table 1. The data have been Hann-smoothed to a velocity resolution of 0.27 km s^{-1} and the integration time on source was 3.83 h. (c) The OH 1667 line for position 2 in Table 1. The Gaussian-fit line parameters for this detection are also given in Table 1. The data have been Hann-smoothed to a velocity resolution of 0.27 km s^{-1} and the integration time on source was 4.25 h. (d) The OH 1667 line for position 3 in Table 1. The Gaussian-fit line parameters for this detection are also given in Table 1. The data have been Hann-smoothed to a velocity resolution of 0.27 km s^{-1} and the integration time on source was 3.17 h.

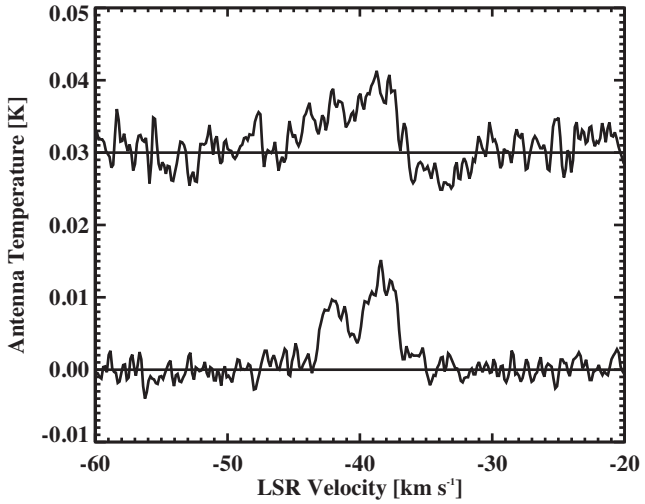

Figure 3. Composite 1665 MHz (top) and 1667 MHz (bottom) spectra for the first four positions in Table 1. The spectra were averaged to reduce the noise and the net integration time was 14.92 h on source. Two components are clearly noticeable in the 1667 MHz line while the 1665 MHz line shows a single broad component. The Gaussian-fit parameters for the two lines are given in Tables 1 and 3. The data were Hann-smoothed to a velocity resolution of 0.27 km s^{-1}.

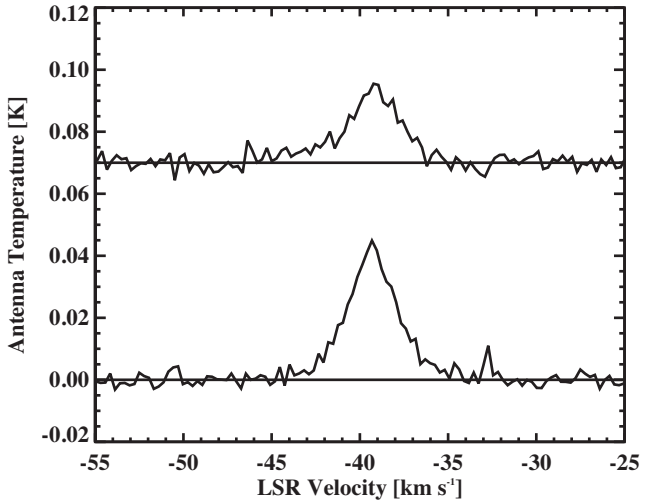

Figure 4. Same as Fig. 3 but for the 'H I peak' position. The integration time here was 25.73 h, and the velocity resolution is virtually the same as for the spectra in Figs 2 and 3.

sight, 0.08 mag, we obtain 4.6×10^{20} cm^{-2}, consistent with Désert et al. (1990) and our OH results, at least for the larger values of T_{ex}.

4.3 The 1665 MHz line

The 1665 MHz line was detected for all lines of sight where we had 1667 MHz emission. However, with the exception of the H I peak observation, the signal-to-noise ratio was only in the 2–3 range. Thus, for the four 1667 MHz detections from the 2016 observing run, we added the 1665 MHz spectra together. The composite spectrum shows a weak, but clear, 1665 MHz signal (see Fig. 3). The parameters for this line and the one at the H I peak are shown in Table 3. For the composite spectrum, the signal-to-noise ratio of the 1665 MHz line does not show two distinct velocity components as does the 1667 MHz line (see Fig. 3), but the extent of the OH emission is virtually the same for both spectra. Although the lines appear qualitatively different, multiplying the 1665 MHz line by 1.8 (the ratio of the 1667/1665 lines in the optically thin approximation) and subtracting one spectrum from the other leaves a noise spectrum with no identifiable features. This implies that the emission from the two transitions is consistent as far as spectral features. For the H I peak detection, the 1665 MHz line shows a possible blueshifted wing. However, once again multiplying the 1665 MHz line by 1.8 and subtracting from the 1667 MHz line spectrum left a residual indistinguishable from noise. Thus, the 1665 MHz line is similar in both instances to the 1667 MHz transition, and there is no sign of anomalous excitation.

The ratio of the integrated intensities (1667/1665) is 1.42 ± 0.39 for the four summed detections and 1.86 ± 0.15 for the H I peak. This indicates the OH 18 cm main lines arise in optically thin gas (e.g. Wouterloot 1981) and is not surprising given the low column densities in the cloud.

5 DISCUSSION

5.1 Mass and gravitational state

We can assess the gravitational stability of G211+63 by comparing the mass of the cloud derived from our estimates of N(H_2) from *Section* 4 to the virial mass derived from the velocity dispersion of the detections listed in Table 1. We begin with the determination of the virial mass. For a sphere with uniform density, the virial theorem gives

$$\sigma_{1D} = 0.0293(M_{vir}/R)^{0/5} \text{ km s}^{-1}, \quad (2)$$

where σ_{1D} is the one-dimensional velocity dispersion in km s^{-1}, M_{vir} is the virial mass in solar masses, and R is the equivalent radius in pc from the projected surface area: $R = (\Omega d^2)^{0.5}$, with Ω as the solid angle covered by the cloud and d the distance from the Sun. We estimate Ω from the area within the 0.08 mag $E(B-V)$ contour in Fig. 1 to be ≈ 0.11 deg^2 ≈ 3.4×10^{-5} steradians. For the cloud distance, Désert et al. (1990) estimate that G211+63 is at 100 pc. This is based primarily on observations of calcium absorption lines by Wesselius & Fejes (1973) who bracketed the nearby IVC neutral hydrogen complex NHX 210° + 70° − 42 between 12 and 400 pc. G211+63 is projected on the periphery of this larger H I structure and likely shares its distance. We will determine the mass of G211+63 on the basis of four possible distances: 100, 200, 300, and 400 pc.

The seven LSR velocities in Table 1 give $\sigma_{1D} = 1.53$ km s^{-1} allowing us to determine the virial mass of G211+63 using equation (2). The values for M_{vir} for the four possible distances are given in Table 4. We also calculate M_{vir} for a cloud density distribution $\rho \propto R^{-2}$ using the standard relationship

$$M_{vir} = 393\sigma_{1D}^2 R \text{ M}_\odot. \quad (3)$$

As is clear from Table 4, the lowest reasonable virial mass is 530 M$_\odot$. We can estimate the mass of G211+63 from our OH data by using the data in Table 2, assuming a cloud distance and an OH/H_2 ratio. If the cloud has an area of 3.4×10^{-5} steradians, this becomes 3.3×10^{36} cm^2 at 100 pc. Expressing $M(\text{OH}) = N(\text{OH})\, A\, m_{OH}$ – where m_{OH} is the mass of an OH molecule in grams (2.8×10^{-23} g), A is the area in cm^2, and N(OH) is the average OH column density at $T_{ex} = 5$ K (the highest column densities from Table 2) in the given area – we derive an OH mass for the cloud of 1.0×10^{28} g for a cloud distance of 100 pc and 16 times more than that for a distance of 400 pc. If we assume an OH/H_2

Table 2. OH column densities for four possible excitation temperatures.

Position	N(OH) for $T_{ex} = 5$ K (cm^{-2})	N(OH) for $T_{ex} = 10$ K (cm^{-2})	N(OH) for $T_{ex} = 20$ K (cm^{-2})	N(OH) for $T_{ex} = 30$ K (cm^{-2})
CO peak	$3.20 \pm 1.78 \times 10^{13}$	$1.62 \pm 0.90 \times 10^{13}$	$1.30 \pm 0.73 \times 10^{13}$	$1.22 \pm 0.68 \times 10^{13}$
Position 1[a]	$1.54 \pm 0.33 \times 10^{14}$	$7.84 \pm 1.67 \times 10^{13}$	$6.29 \pm 1.34 \times 10^{13}$	$5.90 \pm 1.26 \times 10^{13}$
Position 2[a]	$1.22 \pm 0.23 \times 10^{14}$	$6.18 \pm 1.16 \times 10^{13}$	$4.96 \pm 0.93 \times 10^{13}$	$4.66 \pm 0.87 \times 10^{13}$
Position 3[a]	$8.45 \pm 4.19 \times 10^{13}$	$4.29 \pm 2.13 \times 10^{13}$	$3.44 \pm 1.71 \times 10^{13}$	$3.23 \pm 1.60 \times 10^{13}$
H I peak	$1.59 \pm 0.20 \times 10^{14}$	$8.08 \pm 1.03 \times 10^{13}$	$6.49 \pm 0.83 \times 10^{13}$	$6.09 \pm 0.78 \times 10^{13}$
Average	$1.10 \pm 0.64 \times 10^{14}$	$5.60 \pm 3.25 \times 10^{13}$	$4.50 \pm 2.60 \times 10^{13}$	$4.22 \pm 2.44 \times 10^{13}$

[a]Separate components from Table 1 are added together here.

Table 3. 1665 MHz line data.

Position	T_A (mK)	Δv(FWHM) ($km\,s^{-1}$)	v_{LSR} ($km\,s^{-1}$)	W_{OH}^a ($mK\,km\,s^{-1}$)	$W_{OH}(1667)/W_{OH}(1665)$
Total four detections[b, c]	9.2 ± 2.2	2.44 ± 0.58	−38.44	24.0 ± 8.1	1.68 ± 0.62
_[b, c]	5.9 ± 2.2	3.89 ± 1.45	−42.16	24.4 ± 12.9	0.95 ± 0.54
_[b, d]	7.9 ± 2.2	5.27 ± 1.33	−40.18	44.6 ± 16.8	1.42 ± 0.39
H I peak	23.0 ± 2.1	3.21 ± 0.29	−39.06 ± 0.08	79.0 ± 10.1	1.86 ± 0.15

[a]W_{OH} is defined as $\int T_A\, dv$.
[b]Data are Hann-smoothed to 0.27 $km\,s^{-1}$ resolution.
[c]Two Gaussians fit to data.
[d]Single Gaussian fit to data.

ratio of 1.0×10^{-7} as described in Section 4.2, these values become 51–820 $M_\odot$. Values of N(OH) for 10–30 K give lower masses. Only the highest possible cloud mass ($T_{ex} = 5$ K, $d = 400$ pc) is greater than the lowest plausible virial mass (density $\propto R^{-2}$, $d = 100$ pc). All other values of T_{ex} and d lead to lower cloud masses compared to the virial mass. If we compare masses at the same distance, then the virial mass of the cloud is at least 2.6 times the mass derived from the OH observations.

An alternate way to analyse the gravitational state of the cloud is to follow Magnani, LaRosa & Shore (1993) and use the column density of a Jeans-unstable clump, $N_J = n\lambda_J$, where λ_J is the Jeans length. N_J can be written as

$$N_J = 2 \times 10^{22} v_{5,t}\, n_3^{1/2} \mu^{-1/2}\ \ cm^{-2}, \quad (4)$$

where n_3 is the number density of the gas in units of 1000 cm^{-3}, $v_{5,t}$ is the turbulent velocity (approximated here as the velocity dispersion of the cloud) in $km\,s^{-1}$, and μ is the mean molecular weight that we will assume to be 2.3 for a gas composed of H_2 and He. The cloud is gravitationally unstable to collapse if $N \geq N_J$. The volume density can be obtained from Table 2 by taking the average column density, multiplying by the inverse of the OH/H_2 abundance, and dividing by the path length through the cloud. If we assume the cloud extends in the radial direction, the same amount as in the plane of the sky, the path length would be ≈1–4 pc for distances ranging from 400 to 100 pc. In the most extreme low column density case ($T_{ex} = 30$ K), n has a value of 34–140 cm^{-3}. All other values of T_{ex} lead to higher average densities. For these estimates of n, N_J ranges from 3.7 to 7.5 × 10^{21} cm^{-2}. The highest column density derivable from the OH data in Table 2 is based on $T_{ex} = 5$ K. Using this value and the OH/H_2 abundance leads to an average $N(H_2)$ of 1.1×10^{21}. Even comparing the highest cloud column densities with the lowest values of N_J leads to the conclusion that the cloud is not gravitationally collapsing.

In this respect, G211+63 resembles the bulk of high-latitude molecular clouds that are not bound by gravity and likely breaking up on the sound crossing time (∼10^6 yr). If this analysis is confirmed for other IVMCs then these objects may be transient structures formed as thermal instabilities in large-scale atomic flows (e.g. Shore et al. 2003; Shore et al. 2007; Barriault et al. 2010b).

5.2 Linewdiths compared to CO

Désert et al. (1990) observed only one position in the cloud (which we refer to as the 'CO peak') in the CO(1–0) line. They noted one component with a velocity full width at half-maximum (FWHM) of 1.9 $km\,s^{-1}$. They also reported other CO observations but of the (2–1) line from the IRAM 30 m radio telescope that showed two distinct velocity components like the ones we observe for positions 1–3. They give no line parameters but comment that the strength of the two peaks was highly variable within two beams (about 30 arcsec) of the central observation at $(\ell, b) = (210.927°, 63.280°)$. They do show a spectrum for the central CO(2-1) position where the two components are each only two channels wide. Their IRAM observations were made at 1.3 $km\,s^{-1}$ resolution so the individual components have to be less than 2.6 $km\,s^{-1}$ wide (FWHM). Our OH linewidths are clearly larger than the CO lines in four out of seven instances.

The reason for this behaviour is difficult to ascertain because the CO and OH observations are at significantly different sensitivities and resolutions. The behaviour of molecular gas at cloud edges is not often discussed and there is little consensus on even the phenomenology of spectral lines at cloud edges. If the OH main lines are tracing the diffuse outer regions of the molecular cloud, then the broader profiles could be due to two effects: (1) The portion of line coming from the cloud edge could be tracing gas at significantly lower density than along the ridge. This gas might be more easily 'stirred up' by external flows than the denser, more sheltered inner regions of the cloud. (2) Alternatively, intermittency could play a role in broadening the profile (Falgarone et al. 1994; Falgarone & Phillips 1990). Normally, intermittency is demonstrated as non-Gaussian wings on a probability distribution function (PDF) – in this case the PDF is a histogram of the fluctuations of velocity centroids

Table 4. Virial and OH-derived masses for G211+63 as a function of distance.

Distance (pc)	R (pc)	$M^a_{\rm vir}$ ($M_\odot$)	$M^b_{\rm vir}$ ($M_\odot$)	M at 5 K ($M_\odot$)	M at 10 K ($M_\odot$)	$M^b_{\rm vir}$ / (M at 5 K)	$M^b_{\rm vir}$ / (M at 10 K)
100	0.58	1.6×10^3	5.3×10^2	51	26	10	20
200	1.16	3.3×10^3	1.1×10^3	200	100	5.5	11
300	1.75	4.8×10^3	1.6×10^3	460	230	3.5	7.0
400	2.33	6.4×10^3	2.1×10^3	820	420	2.6	5.0

[a]Assumes uniform density.
[b]Assumes density $\propto R^{-2}$.

as obtained from individual spectra across the face of a cloud. However, Magnani & Shore (2017) argue that for homogeneous turbulence, this should be the same as the line profile, where we substitute the fluctuations along the radial direction through the cloud for the fluctuations across the face of the cloud. In this sense, our more sensitive spectra might allow us to see intermittency if it is present along the line of sight. From the Gaussian fits to the data (Tables 1 and 3), it seems that the profiles are well fit by a Gaussian distribution. The blueshifted 'wing' in the 1665 MHz profile from the H I peak is most likely not real, especially as it is not seen in the 1667 MHz line. Either intermittency is not present along the observed lines of sight (this could be a consequence of the turbulence not being fully developed) or the data are not sensitive enough to pick up the non-Gaussian portions of the line. If the latter is the case, then given our very long integration times, it would seem the OH 18 cm lines are not the right transitions for detecting intermittency in diffuse or translucent molecular clouds. Thus, the lack of non-Gaussian wings in the 1667 MHz line at the H I peak seems to indicate that the transition is tracing molecular gas that arises from the stirred-up edges of the cloud.

6 SUMMARY

We present the first observations of the OH main lines at 18 cm in an IVMC. The cloud, G211+63, was observed in seven lines of sight along an infrared ridge that seems to define the molecular portion of the cloud. We detected OH emission in five of them and these are the first OH detections in this type of molecular cloud. All of the detections have $E(B-V) \approx 0.08$–0.09 mag supporting recent claims that the OH 1665 and 1667 MHz lines are excellent tracers of diffuse molecular gas. The strongest emission we detected came from the lower portion of the infrared ridge away from the dust peak. This observation was at a very high sensitivity ($T_{\rm rms} \approx 2$ mK) and the 1665 MHz line was clearly detected with a 1667/1665 line ratio of 1.86 ± 0.15, consistent with optically thin emission. The column densities we calculated from our data range from 1.2 to 15.9×10^{13} cm^{-2} for excitation temperatures ranging from 5 to 30 K. Under the assumption that the OH/H_2 ratio is 1.0×10^{-7}, the resulting molecular column densities are consistent with both $E(B-V)$ values for G211+63 from the Schlegel et al. (1998) data base and with estimates from CO data presented by Désert et al. (1990).

By estimating the size of the cloud as the region with $E(B-V) \geq 0.08$ mag, we determine the cloud mass to range from 26 to 820 $M_\odot$ for distances from 100 to 400 pc and $T_{\rm ex}$ from 5 to 10 K. We also used our limited OH data to determine a velocity dispersion for the cloud of 1.53 km s^{-1}. With this value we then determine that the cloud mass is significantly less than the virial mass. If this result is corroborated by more extensive mapping in either OH or CO, then the cloud would be breaking up on a sound crossing time-scale ($\sim 10^6$ yr). The results of our observations indicate that G211+63 most closely resembles diffuse molecular clouds such as those catalogued by Magnani et al. (1996).

ACKNOWLEDGEMENTS

We thank the Arecibo Observatory telescope operators for expertly setting up our remote observations, and Prof. Steve Shore and an anonymous referee for comments.

REFERENCES

Allen R. J., Ivette Rodríguez M., Black J. H., Booth R. S., 2012, AJ, 143, 97
Allen R. J., Hogg D. E., Engelke P. D., 2015, AJ, 149, 123
Barriault L., Joncas G., Lockman F. J., Martin P. G., 2010a, MNRAS, 407, 2645
Barriault L. et al., 2010b, MNRAS, 406, 2713
Bloemen J. B. G. M. et al., 1986, A&A, 154, 25
Bohlin R. C., Savage B. D., Drake J. F., 1978, ApJ, 224, 132
Cotten D. L., Magnani L., Wennerstrom E. A., Douglas K. A., Onello J. S., 2012, AJ, 144, 163
Dame T. M., Hartmann D., Thaddeus P., 2001, ApJ, 547, 792
Désert F. X., Bazell D., Blitz L., 1990, ApJ, 355, L51
Donate E., Magnani L., 2017, MNRAS, 472, 3169
Falgarone E., Phillips T. G., 1990, ApJ, 359, 344
Falgarone E., Lis D. C., Phillips T. G., Pouquet A., Porter D. H., Woodward P. R., 1994, ApJ, 436, 728
Grenier I. A., Casandjian J.-M., Terrier R., 2005, Science, 307, 1292
Grossmann V., Meyerdierks H., Mebold U., Heithausen A., 1990, A&A, 240, 400
Heiles C., Reach W. T., Koo B.-C., 1988, ApJ, 332, 313
Hollenbach D. J., Tielens A. G. G. M., 1997, ARAA, 35, 79
Kuntz K. D., Danly L., 1996, ApJ, 457, 703
Langer W. D., Velusamy T., Pineda J. L., Goldsmith P. F., Li D., Yorke H. W., 2010, A&A, 521, L17
Langer W. D., Velusamy T., Pineda J. L., Willacy K., Goldsmith P. F., 2014, A&A, 561, 122
Liszt H., Lucas R., 2002, A&A, 391, 693
Lucas R., Liszt H., 1996, A&A, 307, 237
Magnani L., Onello J. S., 1993, ApJ, 408, 559
Magnani L., Shore S. N., 2017, A Dirty Window. Springer-Verlag, GmbH Germany
Magnani L., Smith A. J., 2010, ApJ, 722, 1685
Magnani L., Blitz L., Mundy L., 1985, ApJ, 295, 402
Magnani L., LaRosa T. N., Shore S. N., 1993, ApJ, 402, 226
Magnani L., Hartmann D., Speck B. G., 1996, ApJS, 106, 447
Mebold U., Cernicharo J., Velden L., Reif K., Crezelius C., Goerigk W., 1985, A&A, 151, 427
Meng S. Y., Kraus J. D., 1970, AJ, 75, 535
Reach W. T., Koo B.-C., Heiles C., 1994, ApJ, 429, 672
Richter P., Wakker B., Savage B., Sembach K., 2003, ApJ, 586, 230
Schlafly E., Finkbeiner D. P., 2011, ApJ, 737, 103
Schlegel D. J., Finkbeiner D. P., Davis M., 1998, ApJ, 500, 525

Shore S. N., Magnani L., LaRosa T. N., McCarthy M. N., 2003, ApJ, 593, 413
Shore S. N., LaRosa T. N., Magnani L., Chastain R. J., Costagliola F., 2007, in Elmegreen B. G., Palous J., eds, Proc. IAU Symp. 237, Triggered Star Formation in a Turbulent ISM., Cambridge University Press, Cambridge, p. 17
Smith A. J., 2018, PhD thesis, Univ. Georgia
van Dishoeck E. F., Black J. H., 1988, ApJ, 334, 771
Verschuur G. L., 1971, AJ, 76, 317
Wakker B. P., 2006, ApJS, 163, 282
Wannier P. G., Andersson B.-G., Federman S. R., Lewis B. M., Viala Y. P. , Shaya E., 1993, ApJ, 407, 163
Weselak T., Galazutdinov G. A., Beletsky Y., Krelowski J., 2010, MNRAS, 402, 1991
Wesselius P. R., Fejes I., 1973, A&A, 24, 15
Wolfire M. G., Hollenbach D., McKee C. F., 2010, ApJ, 716, 1191
Wouterloot J. G. A., 1981, PhD thesis, Leiden Observatory

This paper has been typeset from a TEX/LATEX file prepared by the author.